Langmuir
Article
pubs.acs.org/Langmuir


# Solution Self-Assembly and Adsorption at the Air−Water Interface of the Monorhamnose and Dirhamnose Rhamnolipids and Their Mixtures

M. L. Chen,[†] J. Penfold,*[,†,‡] R. K. Thomas,[†] T. J. P. Smyth,[§] A. Perfumo,[§] R. Marchant,[§] I. M. Banat,[§] P. Stevenson,[∥] A. Parry,[∥] I. Tucker,[∥] and I. Grillo[⊥]

[†]*Physical and Theoretical Chemistry Department, University of Oxford, South Parks Road, Oxford, U.K.,* [‡]*STFC, Rutherford Appleton Laboratory, Chilton, Didcot, OXON, U.K.,* [§]*School of Biomedical Sciences, University of Ulster, Coleraine, Northern Ireland,* [∥]*Unilever Research and Development Laboratory, Port Sunlight, Wirral, U.K., and* [⊥]*Institute Laue Langevin, 6 rue Jules Horowitz, F-38042 Grenoble, Cedex 09, France*

*Received August 10, 2010. Revised Manuscript Received October 4, 2010*

The self-assembly in solution and adsorption at the air−water interface, measured by small-angle neutron scattering, SANS, and neutron reflectivity, NR, of the monorhamnose and dirhamnose rhamnolipids (R1, R2) and their mixtures, are discussed. The production of the deuterium-labeled rhamnolipids (required for the NR studies) from a *Pseudomonas aeruginosa* culture and their separation into the pure R1 and R2 components is described. At the air−water interface, R1 and R2 exhibit Langmuir-like adsorption isotherms, with saturated area/molecule values of about 60 and 75 Å$^2$, respectively. In R1/R2 mixtures, there is a strong partitioning of R1 to the surface and R2 competes less favorably because of the steric or packing constraints of the larger R2 dirhamnose headgroup. In dilute solution ($<20$ mM), R1 and R2 form small globular micelles, $L_1$, with aggregation numbers of about 50 and 30, respectively. At higher solution concentrations, R1 has a predominantly planar structure, $L_\alpha$ (unilamellar, ULV, or bilamellar, BLV, vesicles) whereas R2 remains globular, with an aggregation number that increases with increasing surfactant concentration. For R1/R2 mixtures, solutions rich in R2 are predominantly micellar whereas solutions rich in R1 have a more planar structure. At an intermediate composition (60 to 80 mol % R1), there are mixed $L_\alpha/L_1$ and $L_1/L_\alpha$ regions. However, the higher preferred curvature associated with R2 tends to dominate the mixed R1/R2 microstructure and its associated phase behavior.

## 1. Introduction

A wide variety of biosurfactants are synthesized by many different microorganisms. These include the glycolipids, such as the rhamnolipids, trehalolipids, and sophorolipids, which are in general dissacharides acetylated by long-chain fatty acids. The other major category is the lipopeptides, such as surfactin and hydrophobin, which are strongly surface-active. It is difficult to generalize about their biological function, but most play a role in bacterial growth and optimizing access to carbon sources, in addition to a wide range of other specialist purposes. In recent years, their production and characterization have received much attention, and a number of comprehensive reviews exist.[1−4] Compared with conventional surfactants, their lower toxicity, higher biogradability, higher tolerance to pH, temperature, and salinity, and their ability to be synthesized from a variety of nonpetrochemical sources have increased their potential attraction. However, this has to be set against a greater difficulty in large-scale production and purification. Despite this, they have been applied to an increasingly diverse range of applications, which include enhanced oil recovery,[5] bioremediation,[6] and specialized health care, cosmetic, and food processing areas, which exploit their emulsification or antimicrobial/antifungal properties.[7] The other major limitation in their wider application and exploitation is the lack of fundamental physicochemical studies and characterization of the different biosurfactants and biosurfactant components and their mixing with conventional surfactants. This is the focus of this article, which aims to provide a detailed understanding of the surface adsorption and the solution self-assembly properties of the rhamnolipids from *Pseudomonas aeruginosa*.

The rhamnolipids are produced by different strains of the bacterium *Pseudomonas aeruginosa*[2] and generally exist as one or two molecules of rhamnose linked to one or two molecules of $\beta$-hydroxydecanoic acid. The most common forms are L-rhamnosyl-L-rhamnosyl-$\beta$-hydroxydecanoyl-$\beta$-hydroxydecanoate (Figure 1a) and L-rhamnosyl-$\beta$-hydroxydecanoyl-$\beta$-hydroxydecanoate (Figure 1b), which we abbreviate as $Rha_2C_{10}C_{10}$ (R2) and $RhaC_{10}C_{10}$ (R1), respectively. In practice, a variety of other components of different alkyl chain length combinations, depending upon the carbon source and bacterial strain, exist as minority components.

A limited number of recent publications have addressed different aspects of rhamnolipid surface adsorption and self-assembly, and we briefly review those directly relevant to this study. Abolas et al.[8] reported details of the production, purification, and characterization of rhamnolipids produced from soybean oil refinery waste. They reported surface tension data, critical micellar concentration (cmc) values, and adsorbed amounts for R1/R2 mixtures.

(1) Nitschke, M.; O'Costa, S. G. V. A.; Contiero, J. *Biotechnol. Prog.* **2005**, *21*, 1593.
(2) Desai, J. D.; Banat, I. M. *Microbiol. Mol. Biol. Rev.* **1997**, *61*, 47.
(3) Ron, E. Z.; Rosenberg, E. *Environ. Microbiol.* **2001**, *31*, 229.
(4) Muthusamy, K.; Gopalakrishnan, S.; Kochupappy, T.; Sivachidambaram, R.; Sivachidambaram, P. *Curr. Sci.* **2008**, *94*, 736.
(5) Banat, I. M.; Mukkar, R. S.; Cameotra, S. S. *Appl. Microbiol. Biotechnol.* **2000**, *53*, 495.
(6) Milligan, C. N. *Environ. Pollut.* **2005**, *133*, 183.
(7) Singh, P.; Cameotra, S. S. *Trends Biotechnol.* **2004**, *22*, 142.
(8) Abolas, A.; Pinazo, A.; Infante, M. R.; Casals, M.; Garcia, F.; Manresa, A. *Langmuir* **2001**, *12*, 1367.

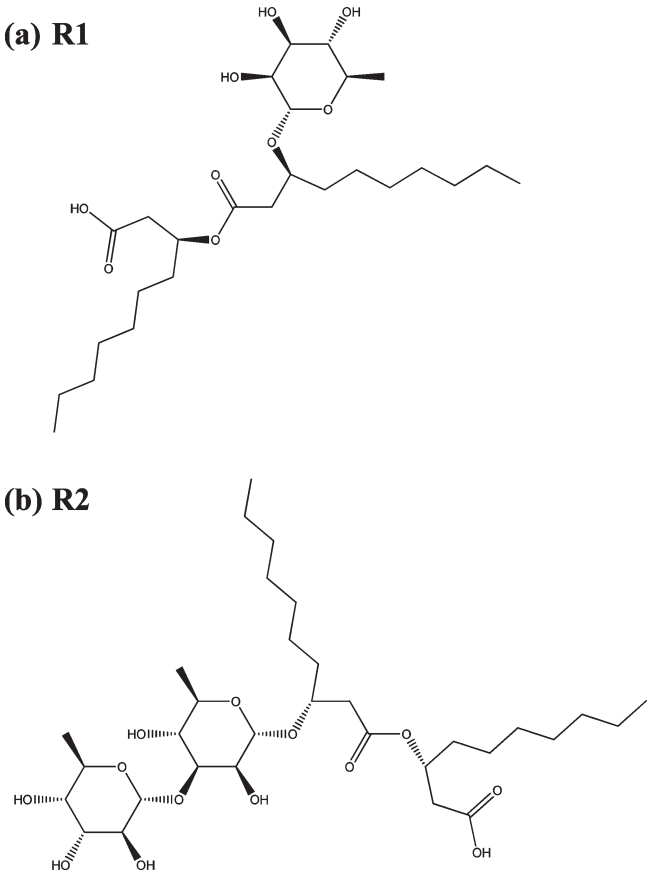


**Figure 1.** Chemical structures of (a) R1 and (b) R2.

Ozdemir et al.[9] reported the pH dependence of the surface and the interfacial behavior of rhamnolipids R1 and R2. They reported decreases in the cmc of $10^{-4}$ and $1.5 \times 10^{-4}$ M at pH 6.8 to $4 \times 10^{-5}$ M for R1 and R2, respectively, at pH 5. Values for the area/molecule at the air−water interface were quoted as varying from about 60 Å$^2$ at pH 5 to about 130 Å$^2$ at pH 6.8, with R1 and R2 having broadly similar values. This was based on the assumption that the prefactor in the Gibbs equation changed from 2 at pH 6.8 to 1 at pH 5. It is assumed that at the higher pH the surfactant is anionic because of the carboxyl groups and is nonionic at the lower pH. In a related study, Helvaci et al.,[10] using the same assumptions about the Gibbs prefactor in evaluating the area/molecule, quantified the decreases in the cmc and area/molecule with the addition of electrolyte. They also reported a transition from micellar to lamellar structures in solution on the addition of electrolyte. From a combination of surface tension, surface rheology, and conductivity, Peker et al.[11] discussed the impact of added rhamnose sugars in solution on the surface behavior and surface structure of R1 and R2. Zhong et al.[12] reported cmc and area/molecule values for R1 and R2 at pH 6.8 of $1.2 \times 10^{-4}$ and $7.0 \times 10^{-5}$ M and 66 and 79 Å$^2$, respectively. Sanchez et al.[13] used SAXS, light scattering, and TEM to study rhamnolipid, R2, self-assembly in solution, reporting a transition from micellar to vesicle structures with increasing surfactant concentration. From surface tension data, they reported cmc and area/molecule values similar to those reported by Ozdemir et al.[9−11] Guo et al.[14] reported similar observations for R1 and R2 from surface tension and dynamic light scattering data. They also discussed the relative surface activity of R1 and R2 and related it to the different monorhamnose and dirhamnose headgroup structures and conformations. Dahrazma et al.[15] used cryo-TEM and SANS to study the effect of pH on rhamnolipid self-assembly. From their data, they concluded that there was a trend with increasing pH from large vesicles to smaller vesicles and ultimately to micelles, with vesicle/micelle coexistence at intermediate pH values.

In this article, we report the use of surface tension and neutron reflectivity to study the adsorption behavior of the R1 and R2 rhamnolipids and their mixtures at the air−water interface. Measurements were made at pH 9, in the presence of buffer, and at natural pH. The neutron reflectivity measurements were made using deuterium-labeled rhamnolipids, R1 and R2, and the production, separation, and purification of R1 and R2, although described more fully elsewhere,[16] are described briefly here. The corresponding solution self-assembly of R1, R2, and R1/R2 mixtures over a wide composition and concentration range is derived from SANS and some complementary dynamic light scattering (DLS) measurements.

## 2. Experimental Details

**(1). Materials.** The hydrogeneous rhamnolipids were obtained from Jeneil Biosurfactant Co. and separated into the pure R1 and R2 components (abbreviated as h-R1 and h-R2) as described below. The deuterated rhamnolipids were grown in a *Pseudomonas aeruginosa* culture and fed with $D_2O$ and d-glycerol, and the procedure for the production and initial extraction and purification is described in detail elsewhere.[16] The pure R1 and R2 components (abbreviated as d-R1 and d-R2) were separated and characterized as described in detail below and were approximately 90% deuterated.

The hydrogeneous rhamnolipids (e.g., Jeneil) and the deuterated rhamnolipids were separated and purified into the separate R1 and R2 components by medium pressure column chromatography. HPLC-MS was used to check the purity of the R1 and R2 components. The medium pressure column chromatography used a $3.6 \times 46$ cm$^2$ glass chromatography tube filled with a silica gel 60 (Merck KGaA, Germany, particle size 40−63 $\mu$m, 230−400 mesh gel) slurry in chloroform. Four grams of rhamnolipid sample per 10 mL of chloroform was loaded into the column, and the column was washed with chloroform at 1 mL/min until the neutral lipids were totally eluted; this was followed by 50:3 and 50:6 v/v mixtures of chloroform/methanol to elute R1 and a 50:20 mixture to elute R2. Twenty milliliter fractions were collected, combined, and dried in a rotary evaporator. The compositions were checked via thin-layer chromatography on silica gel plates using chloroform/methanol/water (65:15:2) as the mobile phase and also by ESI-MS (in negative mode).

HPLC-MS characterization was carried out using an LCQ quadrupole ion-trap mass spectrometer (Finnigan MAT) using the ESI in tandem mass spectrometry mode. The sheath gas flow was set at 65, and the auxiliary gas flow was 35 (arbitrary units). The spray voltage was 3.5 kV, and the capillary temperature was 350 °C. Nitrogen gas was delivered from a Whatman nitrogen generator, with helium damping gas (99.999% purity) present in the ion trap (BOC Medical Gases). Acetonitrile and HPLC water were obtained from BDH. The HPLC used a reverse-phase $C_{18}$ column (Luna 5 $\mu$C$_{18}$, $250 \times 4.6$ mm$^2$, Phenomenex) with a binary gradient mobile phase composed of HPLC-grade water as mobile phase A and acetonitrile as mobile phase B. Different flow and

(9) Ozdemir, G.; Peker, S.; Helvaci, S. S. *Colloids Surf., A* **2004**, *234*, 135.
(10) Helvaci, S. S.; Peker, S.; Ozdemir, G. *Colloids Surf., B* **2004**, *25*, 225.
(11) Peker, S.; Helvaci, S. S.; Ozdemir, G. *Langmuir* **2003**, *19*, 5838.
(12) Zhong, H.; Zeng, G. M.; Liu, J. X.; Xu, X. M.; Yuan, X. Z.; Fu, H. Y.; Huang, G. H.; Liu, Z.; Ding, Y. *Appl. Microbiol. Biotechnol.* **2008**, *79*, 671.
(13) Sanchez, M.; Aranda, K. J.; Espuny, M. J.; Marques, A.; Teruel, J. A.; Manresa, A.; Ortz, A. *J. Colloid Interface Sci.* **2007**, *307*, 246.
(14) Guo, Y. P.; Hu, Y. Y.; Gu, R. R.; Lu, H. *J. Colloid Interface Sci.* **2009**, *331*, 356.
(15) Dahrazma, B.; Mulligen, C. N.; Nieh, M. P. *J. Colloid Interface Sci.* **2008**, *319*, 590.
(16) Smyth, T. J.; et al. *Appl. Microbiol. Biotechnol.* **2010**, *87*, 1347.

composition conditions were used for the deuterated and hydrogenated rhamnolipids. For the h-rhamnolipids, the initial solvent proportions were 35% A and 65% B, adjusted in a linear gradient to 10% A and 90% B over 15 min and back to 35% A/65% B in 18 min and held for 2 min. The flow rate was 0.5 mL/min, and an injection volume of 20 $\mu$L was used throughout. For the d-rhamnolipids, the initial solvent proportions were 70% A/30% B, adjusted in a linear gradient to 30% A/70% B over 50 min and then back to 70% A/30% B in 55 min and held for 5 min. The same flow rates and volumes were used.

The aqueous solutions of the rhamnolipids were prepared by weight in UHQ water (for the surface tension measurements), in $D_2O$ (for the SANS measurements), and in null reflecting water (nrw, a 92 mol % $H_2O$/8 mol % $D_2O$ mixture) or in $D_2O$ (structural measurements) for the NR measurements. The NR measurements were made at natural pH and at pH 9, and the SANS measurements were made at pH 9. The pH 9 buffer consisted of 0.023 M borax and 0.008 M HCl. The surface tension measurements were made in pure water at pH 7 and 9 and in 0.5 M NaCl. The pH 7 buffer consisted of 0.063 M $K_2PO_4$ and 0.037 M NaOH.

**(2). Surface Tension.** The surface tension measurements were made using a Kruss K10 maximum pull tensiometer with a Pt/Ir du Nouy ring. The tensiometer was calibrated by measurements in pure water before each set of measurements. The measurements were carried out at 30 °C and were made after dipping the Pt/Ir ring in the solution and keeping it at the surface for 15 min to establish equilibrium conditions. The average of three repeated measurements was taken, and the experimental deviation was on the order of $\pm 0.5$ mN m$^{-1}$. The Pt/Ir ring and all associated glassware were washed in chromic acid, deionized water, and acetone. In addition, the Pt/Ir ring was flame dried immediately before each use.

**(3). Neutron Reflectivity.** The neutron reflectivity measurements were made on the SURF reflectometer at the ISIS pulsed neutron source.[17] The measurements were made using a single detector at a fixed angle, $\theta$, of 1.5° and for neutron wavelengths, $\lambda$, in the range of 0.5 to 6.8 Å to provide a wave vector transfer, $Q$, ($Q = {}^{4\pi}/_{\lambda} \sin \theta$, where $\theta$ is the grazing angle of incidence) range of 0.048 to 0.5 Å$^{-1}$. The absolute reflectivity is calibrated with respect to the reflectivity of $D_2O$, and the background is determined from the reflectivity in the limit of high $Q$ using well-established experimental procedures.[18] In the kinematic approximation,[19] the specular reflectivity is related to the square of the Fourier transform of the scattering length density profile, $\rho(z)$,

$$R(Q) = \frac{16\pi^2}{Q^2}\left|\int \rho(z) e^{-iQz}\, dz\right|^2 \qquad (1)$$

where $\rho(z) = \Sigma_i\, n_i(z) b_i$, $n_i(z)$ is the number density of the $i$th nucleus at a distance of $z$ from the interface, and $b_i$ is its scattering length. The application of this technique to the study of surfactant adsorption relies on the ability to manipulate $\rho(z)$ by hydrogen/deuterium (H/D) isotopic substitution, and this has been extensively exploited at the air−water interface for a range of surfactants and mixed surfactants.[19] The analysis of the reflectivity data proceeds using eq 1 or the more complete optical matrix method[19] to calculate the reflectivity from appropriate models.

**(4). SANS.** The SANS measurements were made on the D22 and D11 diffractometers at ILL, France[20] and on the LOQ diffractometer at ISIS, U.K.[21] On D22, the measurements were made at a neutron wavelength, $\lambda$, of 8 Å, a $\Delta\lambda/\lambda$ of 10%, and two different sample-to-detector distances, 3.5 and 16.5 m, to cover a scattering vector, $Q$, range of 0.002 to 0.2 Å$^{-1}$ (where $Q = {}^{4\pi}/_{\lambda} \sin {}^{\theta}/_{2}$ and $\theta$ is the scattering angle). The D11 measurements were made at a neutron wavelength, $\lambda$, of 6 Å, a $\Delta\lambda/\lambda$ of 10%, and three sample-to-detector distances, 1.1, 5.0, and 16.5 m, to cover a $Q$ range of 0.003 to 0.25 Å$^{-1}$. On LOQ, the measurements were made using the white beam time-of-flight method with neutron wavelengths in the range of 2 to 10 Å and a sample-to-detector distance of 4 m to cover a $Q$ range of 0.008 to 0.25 Å$^{-1}$. All the LOQ measurements were made with an 8-mm-diameter beam and on D11 and D22 using a beam of $7 \times 10$ mm$^2$. The data were corrected for background scattering, detector response, and spectral distribution of the incident beam (for LOQ) and were converted to an absolute scattering cross section, $d\sigma/d\Omega$ (cm$^{-1}$), using standard procedures.[22,23]

The form of the SANS scattering patterns ($Q$ dependence) was used qualitatively to identify the lamellar (vesicle), micellar, and mixed-phase regions of the overall phase behavior. In the purely micellar regions, detailed quantitative analysis was also carried out using standard modeling procedures for mixed surfactant micelles[24] adapted for the rhamnolipids.

The scattering from globular surfactant micelles in aqueous solution is described by the decoupling approximation, derived by Hayter and Penfold,[24] such that

$$\frac{d\sigma}{d\Omega} = n[S(Q)|\langle F(Q)\rangle_Q|^2 + \langle |F(Q)|^2\rangle_Q - |\langle F(Q)\rangle_Q|^2] \qquad (2)$$

where the averages denoted by $\langle Q\rangle$ are averages over particles size and orientation and $n$ is the micelle number density. The decoupling approximation assumes that for interacting (finite $S(Q)$) globular micelles there is no correlation among position, size, and orientation. $S(Q)$ is the intermicellar structure factor, and $F(Q)$ is the micelle form factor. The micelle structure (form factor, $F(Q)$) is modeled using a standard core-and-shell model[24] for globular micelles. The structure factor, $S(Q)$, which quantifies the intermicellar interactions/correlations, is included using the rescaled mean spherical approximation, RMSA, calculation[25,26] for a repulsive screened Coulombic intermicellar interaction potential, characterized by the surface charge of the micelle, $z$, the Debye−Huckel inverse screening length, $\kappa_{dh}$ (defined in the usual way), and the micelle number density, $n$.

**(5). Light Scattering.** Dynamic light scattering measurements were made using a Malvern PCS8/4700 instrument and a 7132A correlator. Data were collected in triplicate with run times of 120 s, and the individual autocorrelation functions obtained were analyzed using the Contin method to obtain the particle size distributions.[27] The light scattering measurements were used predominantly to reinforce the identification of the mixed lamellar/micellar phase regions and were particularly sensitive to small levels of the larger lamellar (vesicle) component.

## 3. Results and Discussion

**(1). Surface Adsorption.**

(*i*). *Surface Tension.* (*a*). *R1, R2.* Surface tension measurements were made for R1 and R2 in UHQ water, at pH 7 and 9 and in 0.5 M NaCl, where the controlled pH (7 and 9) was established in buffer (Experimental Details). The surface tension data for R1 and R2 are shown in Figure 2a,b.

(17) Penfold, J.; et al. *J. Chem. Soc., Faraday Trans.* **1997**, *93*, 3899.
(18) Lee, E. M.; Thomas, R. K.; Penfold, J.; Ward, R. C. *J. Phys. Chem.* **1989**, *93*, 381.
(19) Lu, J. R.; Thomas, R. K.; Penfold, J. *Adv. Colloid Interface Sci.* **2000**, *84*, 143.
(20) Neutron beam facilities at the high-flux reactor available to users, ILL, Grenoble, France, 1994.
(21) Heenan, R. K.; King, S. M.; Penfold, J. *J. Appl. Crustallogr.* **1997**, *30*, 1140
(22) Ghosh, R. E.; Egelhaaf, S.; Rennie, A. R. ILL Internal Report, ILL98GH14T, **1998**
(23) Heenan, R. K.; King, S. M.; Osborn, R.; Stanley, H. B. RAL Internal Report, RAL-89-128, **1989**.
(24) Hayter, J. B.; Penfold, J. *Colloid Polym. Sci.* **1983**, *261*, 1072.
(25) Hayter, J. B.; Penfold, J. *Mol. Phys.* **1981**, *41*, 109.
(26) Hayter, J. B.; Hansen, J. P. *Mol. Phys.* **1982**, *42*, 651.
(27) Provencher, S. W. *Makromol. Chem.* **1979**, *180*, 201.

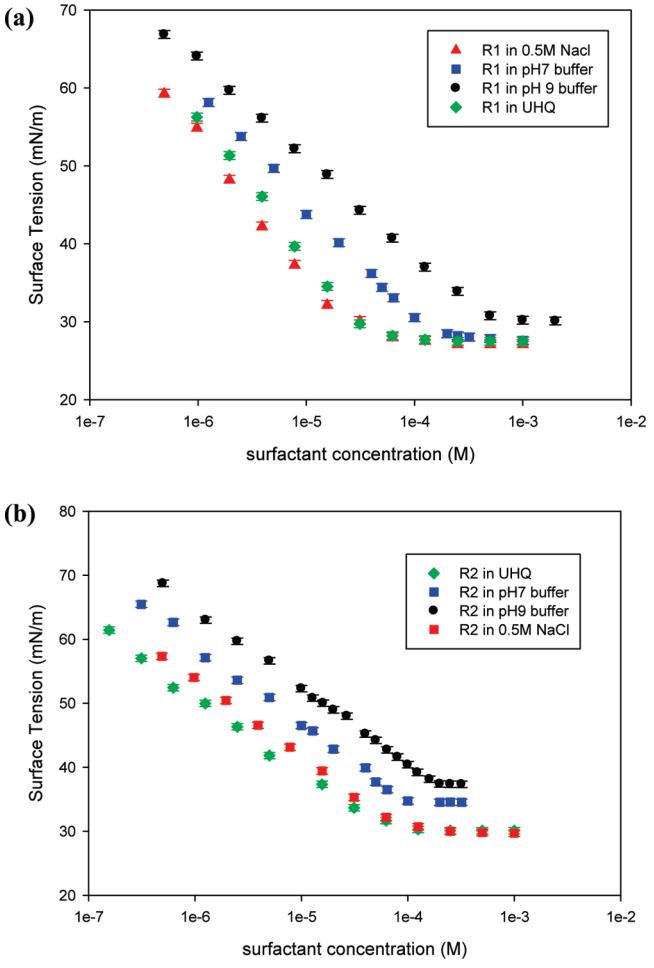


**Figure 2.** (a) Surface tension, $\gamma$, of R1 (pH 7 and 9, UHQ, and 0.5 M NaCl). (b) Surface tension of R2 (pH 7 and 9, UHQ, and 0.5 M NaCl).

The area per molecule (adsorbed amount) at the cmc is obtained from the slope of the $\gamma$ versus ln $C$ curve (where $\gamma$ is the surface tension and $C$ is the solution concentration) below the cmc using the Gibbs equation. The cmc is determined from the intersection of straight-line fits to the surface tension data below and above the cmc. The values of the cmc, area per molecule at the cmc (assuming a Gibbs prefactor of 1.0), and surface tension above the cmc for R1 and R2 are summarized in Table 1.

For R1, with decreasing pH, the area per molecule, cmc, and surface tension value above the cmc all decrease. This is consistent with R1 becoming less ionic and more nonionic as the pH decreases. It is normally assumed that the rhamnolipids are anionic at high pH because of the carboxyl groups but nonionic at low pH. There is little difference between the values for the area/molecule and surface tension above the cmc and only a modest change in the cmc for R1 in UHQ water and in 0.5 M NaCl. This reinforces the assumption that the surfactant is not strongly ionic at the lower pH value, where the addition of this amount of electrolyte would normally result in a more significant decrease in both the cmc and the area per molecule.[28] A similar trend in the variation in the cmc is observed for R2; that is, the cmc decreases with decreasing pH (Figure 1b, Table 1b). However the variation in the area per molecule is less significant and is also not systematic. Furthermore, the addition of 0.5 M NaCl has little impact upon the adsorbed amount or the cmc value. The area per molecule values for R1 and R2 under all of the conditions measured (except at pH 9) are smaller for R1 than for R2. This is consistent with the bulkier dirhamnose headgroup of R2 inhibiting closer packing at the surface, as observed in conventional surfactants such as the polyoxyethylene nonionic surfactants.[29] After comparing the extreme values of the area per molecule for R1 (77 Å$^2$ at pH 9 compared to 53 Å$^2$ in UHQ water) with those for R2 (77 Å$^2$ at pH 7 compared to 84 Å$^2$ in UHQ water), we find that there is a much larger variation in the values for R1 than for R2. The weaker dependence of the area per molecule on pH and on added electrolyte for R2 would imply that R2 behaves even more like a nonionic surfactant than R1. At the lower pH values, the area per molecule values derived from the surface tension are broadly similar to those reported elsewhere in the literature.[8−14] However, at high pH, where different assumptions are made about the Gibbs prefactor, there is a significant discrepancy. We defer any further discussion of the adsorbed amounts until we have presented the NR data, which provides a more direct measure of the surface adsorption. The cmc values measured at the higher and lower pH values are also broadly consistent with literature values.[8−14]

(*b*). *R1/R2*. The surface tension has also been measured for R1/R2 mixtures at pH 9 and at R1/R2 solution compositions of 30/70, 50/50, and 70/30 mol/mol. The key parameters extracted from the surface tension curves are summarized in Table 1c. The quoted area per molecule and adsorbed amounts representing the total adsorption (R1 + R2) assume ideal mixing and a constant Gibbs prefactor of 1.0. The variation in the mixed cmc with solution composition for the R1/R2 mixture is shown in Figure 3. Within experimental error, it shows an almost linear dependence on composition for the pure R1 to pure R2 cmc values. From Clint,[30] the variation of the mixed cmc with composition for ideal mixing should vary as

$$\frac{1}{C^*} = \frac{\alpha}{C_1} + \frac{(1-\alpha)}{C_2} \qquad (3)$$

where $C^*$ is the mixed cmc, $C_1$ and $C_2$ are the cmc's of components 1 and 2 in a binary mixture, and $\alpha$ is the solution composition. The lower dashed line plotted in Figure 3 is calculated using eq 3, assuming $C_1$ and $C_2$ to be correct. Although the data are broadly consistent with the calculation, the general trend is systematically higher. This is not consistent with a negative (synergistic) departure from ideal mixing and would suggest that the mixing behavior is more dominated by R1. The upper dashed line in Figure 3 is a least-squares fit to the data in Figure 3 using eq 4. This provides, within error, a reasonably good description of the data and is consistent with ideal mixing. We have directly measured the variation in surface composition at a fixed surfactant concentration above the cmc using NR. Any further discussion of the detailed nature of the surface mixing is deferred until later in the article.

(*ii*). *Neutron Reflectivity*. (*a*). *R1, R2 Adsorption*. Neutron reflectivity measurements were made at the air−solution interface for the deuterated surfactants (d-R1, d-R2) in nrw (in pure nrw and at pH 9 in buffer, see Experimental Details) at surfactant concentrations from well below the cmc to above the cmc. Under these conditions, the reflected signal arises only from the adsorbed layer of deuterated surfactant at the interface.

(28) van Os, N. M., Haak, J. R.; Rupert, L. A. M. *Physico-Chemical Properties of Selected Anionic, Cationic, and Nonionic Surfactants*; Elsevier: Amsterdam, 1993.

(29) Lu, J. R.; Li, Z. X.; Su, T. J.; Thomas, R. K.; Penfold, J. *Langmuir* **1993**, *9*, 2408.

(30) Clint, J. H. *J. Chem. Soc., Faraday Trans. 1* **1975**, *76*, 1327.

**Table 1. Surface Tension Parameters**

(a) R1

| | surface excess $\Gamma$ ($\pm 0.1 \times 10^{-10}$mol cm$^{-2}$) | area per molecule ($\pm 2$ Å$^2$) | surface tension $\gamma$ ($\pm 0.5$ mN/m) | cmc ($\pm 0.02$ mM) |
|---|---|---|---|---|
| R1 in pH 7 buffer | 2.5 | 66 | 28.7 | 0.18 |
| R1 in pH 9 buffer | 2.2 | 77 | 31.2 | 0.36 |
| R1 in UHQ water | 3.1 | 53 | 27.9 | 0.04 |
| R1 in 0.5 M NaCl UHQ water | 3.2 | 52 | 27.8 | 0.03 |

(b) R2

| | surface excess $\Gamma$ ($\pm 0.1 \times 10^{-10}$mol cm$^{-2}$) | area per molecule ($\pm 2$ Å$^2$) | surface tension $\gamma$ ($\pm 0.5$ mN/m) | cmc ($\pm 0.02$ mM) |
|---|---|---|---|---|
| $R_2$ in pH 7 buffer | 2.2 | 77 | 34.7 | 0.11 |
| $R_2$ in pH 9 buffer | 2.1 | 80 | 37.4 | 0.18 |
| R2 in UHQ water | 2.0 | 84 | 30.3 | 0.07 |
| R2 in 0.5 M NaCl UHQ water | 2.1 | 79 | 30.4 | 0.08 |

(c) R1/R2 Mixtures at 1 mM and pH 9 (in Buffer)

| | surface excess $\Gamma$ ($\pm 0.1 \times 10^{-10}$mol cm$^{-2}$) | area per molecule ($\pm 2$ Å$^2$) | surface tension $\gamma$ ($\pm 0.5$ mN/m) | cmc ($\pm 0.02$ mM) |
|---|---|---|---|---|
| R1/R2 30:70 | 2.0 | 83 | 34.7 | 0.26 |
| R1/R2 50:50 | 2.1 | 78 | 33.5 | 0.34 |
| R1/R2 70:30 | 2.2 | 76 | 32.4 | 0.34 |

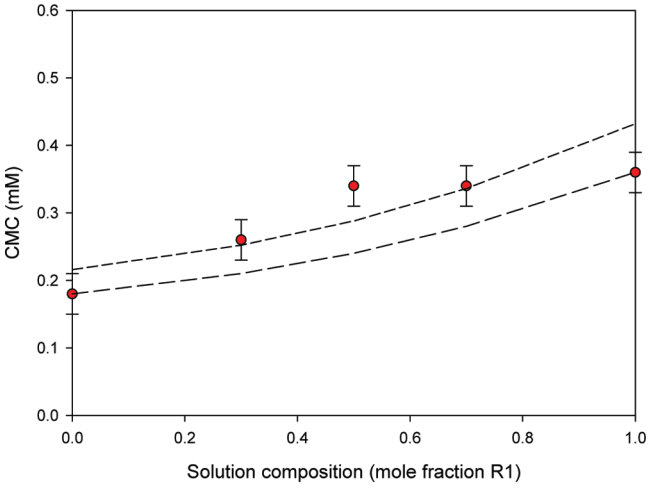


**Figure 3.** cmc variation for the R1/R2 mixture at pH 9 in buffer. The lower dashed line is calculated from eq 4 using the measured cmc values for R1 and R2. The upper dashed curve is a least-squares fit to the cmc data.

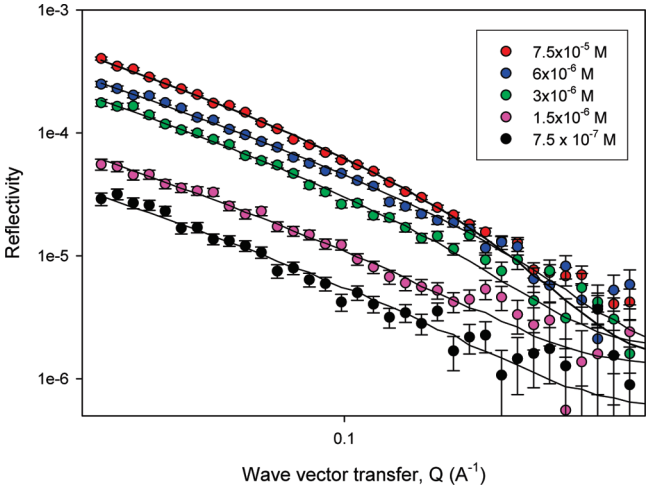


**Figure 4.** Specular reflectivity for R1 in nrw at $7.5 \times 10^{-7}$, $1.5 \times 10^{-6}$, $3 \times 10^{-6}$, $6 \times 10^{-6}$, and $7.5 \times 10^{-5}$ M. The solid lines are model calculations for a single layer of uniform composition and for the parameters in Table 3a.

Typical reflectivity data for d-R1 in nrw at surfactant concentrations of $7.5 \times 10^{-5}$, $6 \times 10^{-6}$, $3 \times 10^{-6}$, $1.5 \times 10^{-6}$, and $7.5 \times 10^{-7}$ M are shown in Figure 4.

In this $Q$ range, the slope of the reflectivity is determined largely by the thickness of the adsorbed layer, and here it is approximately constant over the concentration range illustrated. The absolute level of the reflectivity gives a measure of the adsorbed amount, which decreases as expected with decreasing surfactant concentration. Hence, the reflected signal can be analyzed in terms of the adsorbed amount at the interface and the thickness of the adsorbed layer. The most direct way of determining the adsorption is to assume that the adsorbed layer can be described as a single layer of uniform composition, and this is a good description of the data presented here. The measured reflectivity is then modeled by comparing it with a calculated profile (assessed by least squares) using the optical matrix method[31] for this simple structural model. The model parameters are the scattering length density, $\rho$, and the thickness, $\tau$, of the adsorbed layer and are related to the adsorbed amount or area per molecule, $A$, by[31]

$$\tau\rho = \frac{\sum b}{A} \tag{4}$$

where $\Sigma b$ is the sum of the scattering lengths of the deuterated surfactant, $\Gamma = 1/N_a A$ is the adsorbed amount, and $N_a$ is Avogadro's number.

The solid lines in Figure 4 are model calculations as described above for the parameters in Table 3a and using the scattering lengths tabulated in Table 2.

(31) Penfold, J. In *Neutron, x-Ray and Light Scattering*; Lindner, P., Zemb, T., Eds.; Elsevier: Amsterdam, 1991.

**Table 2. Scattering Lengths and Molecular Volumes for R1, R2, and $D_2O$**

| component | scattering length (Å) | molecular volume (Å$^3$) |
|---|---|---|
| d-R1 | $4.93 \times 10^{-3}$ | 813 |
| h-R1 | $-0.45 \times 10^{-3}$ | 813 |
| d-R2 | $6.02 \times 10^{-3}$ | 1052 |
| h-R2 | $0.64 \times 10^{-3}$ | 1052 |
| $D_2O$ | $1.92 \times 10^{-4}$ | 30 |

**Table 3. Key Model Parameters**

(a) Typical Model Parameters from the Analysis of Neutron Reflectivity Data for d-R1/nrw (Figure 4)

| surfactant concentration (M) | $\tau$ (±1 Å) | $\rho$ (±0.2 × $10^{-6}$ Å$^{-2}$) | $A$ (Å$^2$) | $\Gamma$ (±0.1 × $10^{-10}$ mol cm$^{-2}$) |
|---|---|---|---|---|
| $7.5 \times 10^{-5}$ | 22 | 3.7 | 62 ± 2 | 2.7 |
| $6 \times 10^{-6}$ | 19 | 3.3 | 77 ± 2 | 2.2 |
| $3 \times 10^{-6}$ | 20 | 2.7 | 92 ± 4 | 1.8 |
| $1.5 \times 10^{-6}$ | 21 | 1.5 | 160 ± 10 | 1.1 |
| $7.5 \times 10^{-7}$ | 25 | 0.9 | 215 ± 10 | 0.8 |

(b) Key Model Parameters from the Analysis of Reflectivity Data for R1 and R2

| sample | $\tau$ (±1 Å) | $\rho$ (±0.2 × $10^{-6}$ Å$^{-2}$) | $A$ (Å$^2$) | $\Gamma$ (±0.1 × $10^{-10}$ mol cm$^{-2}$) |
|---|---|---|---|---|
| 1.2 mM 50/50 d-R2/h-R2 | 20 | 2.1 | 72 ± 2 | 2.3 |
| 1.2 mM d-R2 | 23 | 3.5 | 77 ± 2 | 2.2 |
| 0.3 mM d-R1 | 22 | 3.6 | 62 ± 2 | 2.7 |
| 0.3 mM 50/50 d-R1/h-R1 | 21 | 1.7 | 61 ± 2 | 2.8 |

Broadly similar reflectivity profiles to those of R1 are obtained for R2, with and/or without buffer (at pH 9 in buffer). For both surfactants over the concentration range measured, the mean thickness of the adsorbed monolayer is about 21 ± 1 Å.

Measurements on an equimolar mixture of the deuterated and hydrogenated surfactants provide a stringent test of the purity of the surfactants. The model parameters in Table 3b illustrate this for 0.3 mM R1 and for 1.2 mM R2, where the deuterated surfactant and the 50/50 mixture of deuterated and hydrogenated surfactants give, within error, the same adsorption at the interface.

The resulting adsorption isotherms for R1 and R2, without and with buffer (pH 9), are plotted in Figure 5a,b.

The adsorption isotherms have a concentration dependence that is consistent with a Langmuir isotherm of the form

$$\Gamma = \Gamma_{max}\frac{C}{(C+k)} \quad (5)$$

where $\Gamma$ and $\Gamma_{max}$ are the adsorbed amount and the maximum adsorption, $C$ is the surfactant concentration, and $k$ is the adsorption coefficient. This is illustrated in Figure 5c, where the adsorption data for R1 in the absence of buffer are fitted with a Langmuir isotherm for $\Gamma_{max} = 2.7 \times 10^{-10}$ mol cm$^{-2}$ and $k = 1.83 \times 10^{-6}$ mol L$^{-1}$.

From the NR data for both R1 and R2, there is little systematic difference between the adsorption isotherms measured in water and at pH 9 in buffer (Figure 5). For R1, the saturation adsorption is about $2.7 \pm 0.1 \times 10^{-10}$ mol cm$^{-2}$ in water, compared with $2.9 \pm 0.1 \times 10^{-10}$ mol cm$^{-2}$ in buffer at pH 9. For R2, the saturation adsorption is slightly larger in the absence of buffer, about $(2.2 \pm 0.1) \times 10^{-10}$ mol cm$^{-2}$ compared with $(1.9 \pm 0.1) \times 10^{-10}$ mol cm$^{-2}$ in buffer at pH 9. Furthermore, the mean adsorption is higher at saturation for R1 than for R2 in both water and at pH 9.

For R2, the earlier surface-tension-derived adsorbed amounts are in good agreement with the more direct absolute values from neutron reflectivity. From neutron reflectivity, the mean value in both water and in buffer at pH 9 is about $2.1 \times 10^{-10}$ mol cm$^{-2}$ compared with $2.0 \times 10^{-10}$ mol cm$^{-2}$ from surface tension data. For R1, the differences between the neutron reflectivity and surface tension values are slightly greater. In water, the neutron reflectivity value is about $2.7 \times 10^{-10}$ mol cm$^{-2}$ compared with $3.1 \times 10^{-10}$ mol cm$^{-2}$ from surface tension data . At pH 9 (in buffer), the neutron reflectivity value is about $2.9 \times 10^{-10}$ mol cm$^{-2}$ compared with the surface tension value of $2.2 \times 10^{-10}$ mol cm$^{-2}$.

The rhamnolipids are expected to be anionic at high pH and more nonionic as the pH decreases because of the protonation of the carboxylic acid groups. The similarities between the adsorbed amounts for both R1 and R2 in water and at pH 9 from the neutron reflectivity suggest that they are only weakly anionic. The surface-tension-derived adsorbed amount was obtained here using a Gibbs prefactor of 1.0, consistent with the surfactants being essentially nonionic or weakly dissociating. This is further reinforced by the lack of change in the adsorption and cmc with the addition of 0.5 M NaCl from the ST data, as described earlier. Using a Gibbs prefactor of 1.0 , we found that the surface-tension- and neutron-reflectivity-derived adsorbed amounts for R2 in both water and buffer are very similar. (See above.) For R1 in water, the adsorbed amount derived from NR and surface tension data are still the same within the error. However, at pH 9 (in buffer) the values from NR and ST are different. This would require the Gibbs prefactor to be greater than 1.0 (but not 2.0) to reconcile these differences, and a value greater than 1.0 would imply partial counterion binding. Gou et al.[14] have argued that the difference in the relative surface activities of R1 and R2 and their pH dependence arises from changes in the conformation and the corresponding interheadgroup interaction of the R1 and R2 headgroups, which more effectively reduces the ionic nature of R2 compared with that of R1. The results presented here are consistent with that argument.

The most noteworthy difference in the adsorption behavior of the different rhamnolipid components is the difference in the absolute values for R1 and R2; the saturation adsorption of R1 is ~40% higher than for R2. This arises because the larger dirhamnose headgroup will impose greater steric (packing) constraints at the interface and the dirhamnose headgroup will also make R2 more hydrophilic. This is similar to what has been observed, for example, in nonionic surfactants,[29] where in that case the area/molecule increases with increasing headgroup ethylene oxide chain length.

(*b*). *R1/R2 Mixed Adsorption*. Neutron reflectivity measurements were also made for the binary R1/R2 mixture at the air−water interface at a fixed solution concentration of 1 mM at pH 9 (in buffer) and as a function of solution composition from R1-rich to R2-rich compositions. Measurements were made for the two isotopic combinations of d-R1/h-R2/nrw and h-R1/d-R2/nrw, where in each case the reflectivity arises predominantly from the deuterated component at the interface. The reflectivity data can be described as a single layer of uniform composition and analyzed in the way discussed earlier. For the binary mixture, the adsorbed amount of each component can be calculated from[19,31]

$$\rho\tau = \sum\frac{b_1}{A_1} + \sum\frac{b_2}{A_2} \quad (6)$$

where $b_i$ and $A_i$ are the scattering lengths and area/molecule of each component of the binary mixture. Hence, from the reflectivity data for the two different isotopic combinations $A_1$ and $A_2$ can

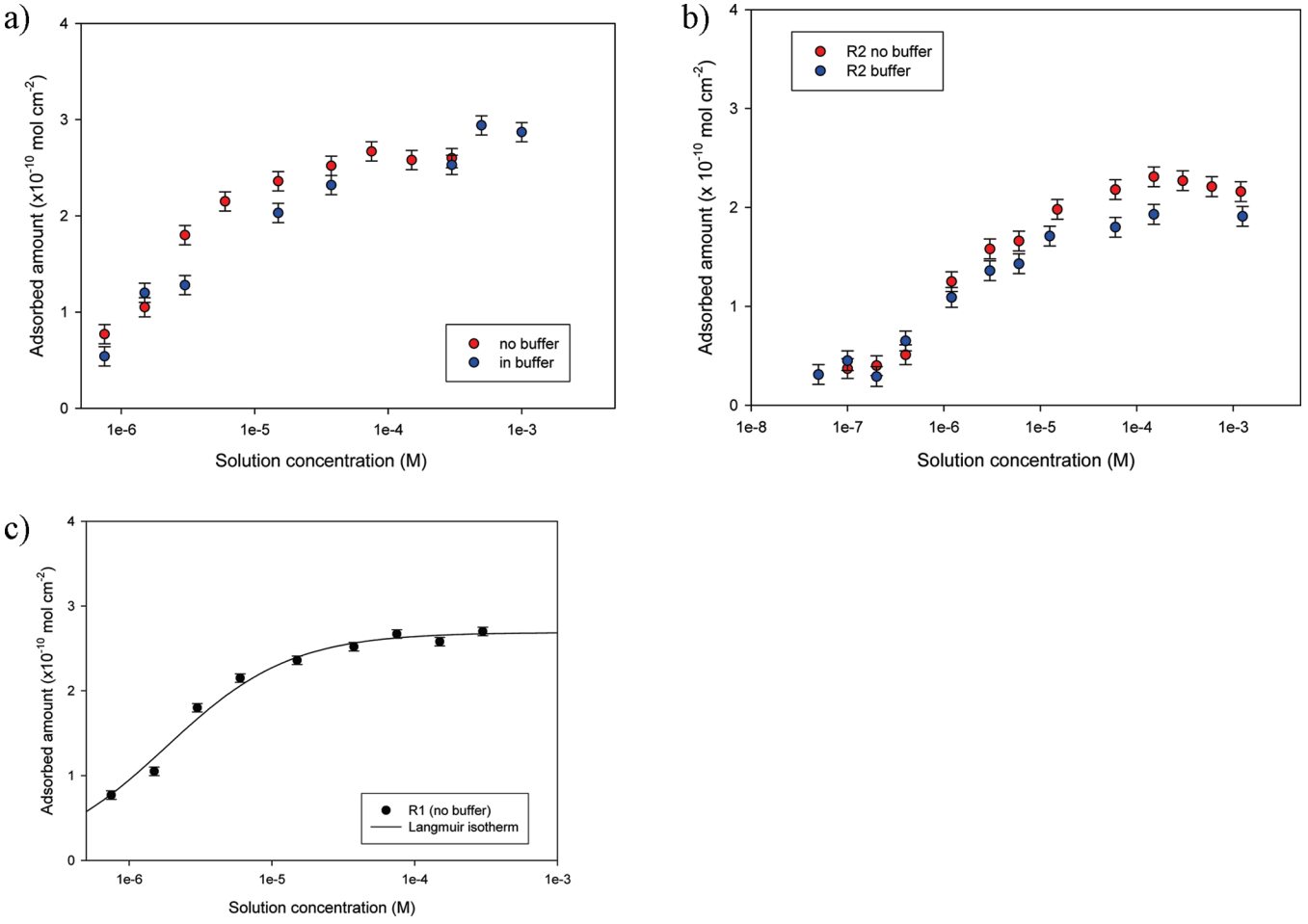


**Figure 5.** Adsorption isotherms for (a) R1 and (b) R2 at pH 9 (in buffer). (c) Adsorption isotherm for R1. The solid line is a calculated line, assuming a Langmuir isotherm, for $\Gamma_{max} = 2.7 \times 10^{-10}$ mol cm$^{-2}$ and $k = 1.83 \times 10^{-6}$ mol L$^{-1}$.

be determined. Typical model parameters and values are summarized in Table 4a.

The mean thickness (average over the composition range measured) for the mixed R1/R2 monolayer is about 23 ± 1 Å. In Table 4b, the variations in the adsorbed amount and surface composition for the R1/R2 mixture are summarized, and they are plotted in Figure 6a,b.

The data are broadly qualitatively consistent with what would be expected in conventional mixed surfactants. However, over the entire solution composition range measured here, the surface adsorption is dominated by the more surface-active R1. The quantitative trend is well outside what would be expected from the standard thermodynamic treatments using the pseudophase approximation and in particular regular solution theory, RST,[32] for such mixtures. The measurements were made at a solution concentration of 1 mM, which is about 3 to 5 times greater than the mixed cmc at all compositions (Figure 3). The cmc variation with solution composition, however, implies close to ideal mixing in the micelles, and the cmc values of R1 and R2 are rather similar. Hence, at this solution concentration the surface composition might be expected to be much closer to the aggregate or solution composition.[32] However, as discused for related systems elsewhere[33] such extreme departures from ideal mixing are not consistent with the existing theoretical treatments of nonideality, such as RST.[32] The surface behavior is, however, broadly similar to that reported for the nonionic surfactant mixture of $C_{12}E_3/C_{12}E_8$.[34,35] For the $C_{12}E_3/C_{12}E_8$ mixture, even at solution concentrations much greater than the cmc the surface adsorption is dominated by the more surface-active $C_{12}E_3$. This is an example of where the surface tension is entirely consistent with ideal mixing, but the differences in surface activity and packing constraints, in particular, the steric hindrance of the much larger $EO_8$ headgroup of the $C_{12}E_8$, result in very different surface behavior. Similar arguments apply here to the surface adsorption of the R1/R2 mixtures. That is, the packing constraints imposed by the larger dirhamnose headgroup of R2 mean that R1 dominates the surface mixing, even at solution concentrations well in excess of the cmc.

(*c*). *Surface Structure for R1, R2, and R1/R2 Mixtures.* Detailed structural information on the surfactant monolayer and mixed monolayer have been obtained by a direct method of analysis based on the kinematic approximation,[36] which provides information about the volume fraction distributions of the individually labeled components. Writing the scattering length density profile, $\rho(z)$, from eq 2 in terms of *i* discrete components, we have

$$\rho(z) = \sum_i n_i(z) b_i \qquad (7)$$

(32) Holland, P. M. *Colloids Surf., A* **1986**, *19*, 171.
(33) Tucker, I.; Penfold, J.; Thomas, R. K.; Tildesley, D. *Langmuir* **2009**, *25*, 3924.
(34) Penfold, J.; Staples, E.; Thompson, L.; Tucker, I. *Colloids Surf., A* **1995**, *102*, 127.
(35) Penfold, J.; Staples, E.; Tucker, I.; Thomas, R. K.; Woodling, R.; Dong, C. C. *J. Colloid Interface Sci.* **2003**, *262*, 235.
(36) Lu, J. R.; Li, Z. X.; Smallwood, J.; Thomas, R. K.; Penfold, J. *J. Phys. Chem.* **1995**, *99*, 8233.

**Table 4. Key Model Parameters**

(a) Key Model Parameters from the Analysis of Neutron Reflectivity Data for a 40/60 R1/R2 Mixture at a Concentration of 1 mM and at pH 9

| contrast | $\tau$ (±1 Å) | $\rho$ (±0.2 × $10^{-6}$ Å$^{-2}$) | $A$ (±4 Å$^2$) | $\Gamma$ (±0.2 × $10^{-10}$ mol cm$^{-2}$) |
|---|---|---|---|---|
| dh | 23 | 2.0 | 107 | 1.6 |
| hd | 24 | 1.3 | 200 | 0.9 |

(b) Variation in Adsorbed Amounts and Surface Composition for 1 mM R1/R2 at pH 9 (in Buffer)

| solution composition (mole fraction R1) | $\Gamma_{R1}$ (±0.1 × $10^{-10}$ mol cm$^{-2}$) | $\Gamma_{R2}$ (±0.1 × $10^{-10}$ mol cm$^{-2}$) | $\Gamma_{total}$ (±0.1 × $10^{-10}$ mol cm$^{-2}$) | surface composition (mole fraction R1, ±0.02) |
|---|---|---|---|---|
| 0.85 | 2.4 | 0.4 | 2.8 | 0.85 |
| 0.7 | 2.1 | 0.5 | 2.6 | 0.82 |
| 0.6 | 2.0 | 0.6 | 2.5 | 0.67 |
| 0.5 | 1.8 | 0.7 | 2.4 | 0.72 |
| 0.4 | 1.6 | 0.9 | 2.5 | 0.65 |
| 0.37 | 1.5 | 0.9 | 2.4 | 0.65 |
| 0.3 | 1.4 | 1.0 | 2.3 | 0.59 |
| 0.27 | 1.3 | 1.0 | 2.3 | 0.56 |
| 0.2 | 1.1 | 1.1 | 2.2 | 0.53 |
| 0.17 | 0.9 | 1.3 | 2.2 | 0.42 |
| 0.11 | 0.8 | 1.4 | 2.1 | 0.36 |

where $b_i$ and $n_i(z)$ are the scattering lengths and number density profiles of the different components. From eq 2, this gives

$$R(Q) = \frac{16\pi^2}{Q^2}\left[\sum_i b_i^2 h_{ii} + \sum_i \sum_{j<i} 2b_i b_j h_{ij}\right] \quad (8)$$

The $h_{ii}$ factors are the self-partial structure factors, $h_{ii} = |\hat{n}_{ii}(Q)|^2$. The $h_{ij}$ cross- partial structure factors, $h_{ij}$, are given by $h_{ij}(Q) = Re\{\hat{n}_i(Q)\,\hat{n}_j(Q)\}$, and $n_i(Q)$ is the 1D Fourier transform of $n_i(z)$. The self-partial structure factors relate directly to the distributions of the individual components at the interface, whereas the cross-partial structure factors relate to their relative positions at the interface along the direction ($z$) normal to the interface, as discussed in detail elsewhere.[36] From a series of different reflectivity measurements using differently labeled combinations, the different partial structure factors can be extracted, and this approach has been applied successfully to a range of different systems.[19] For the binary R1/R2 surfactant mixture in water, the scattering length density profile at the interface, $\rho(z)$ (where $z$ is the direction orthogonal to the plane of the interface) can be written as

$$\rho(z) = b_{R1} n_{R1}(z) + b_{R2} n_{R2}(z) + b_s n_s(z) \quad (9)$$

where $b_i$ and $n_i(z)$ are the scattering lengths and number density profiles of the different components (R1, R2, and solvent, respectively). From eq 8, this gives

$$R(Q) = \frac{16\pi^2}{Q^2}[b_{R1}{}^2 h_{R1R1} + b_{R2}{}^2 h_{R2R2} + b_s{}^2 h_{ss} + 2b_{R1} b_{r2} h_{R1R2} + 2b_{R1} b_s h_{R1s} + 2b_{R2} b_s h_{R2s}] \quad (10)$$

Simple analytical functions describe these partial structure factors well under most circumstances.[19,36] The surfactant self-terms are modeled as Gaussian distributions, the solvent distribution is modeled as a tanh function, and the cross terms are calculated analytically from those distributions assuming fixed displacements between the different components at the interface, as described in detail elsewhere.[19,36] From the reflectivity measurements for R1/R2 mixtures at six different isotopic combinations (d-R1/d-R2/nrw, d-R1/h-R2/nrw, h-R1/d-R2/nrw, h-R1/h-R2/$D_2O$, d-R1/h-R2/$D_2O$, and h-R1/d-R2/$D_2O$) measured at a surfactant concentration of 1 mM and a solution composition of 70/30 mol/mol, the six partial structure factors in eq 10 can be extracted, and the resulting volume fraction distributions at the interface for R1, R2, and solvent are plotted in Figure 7.

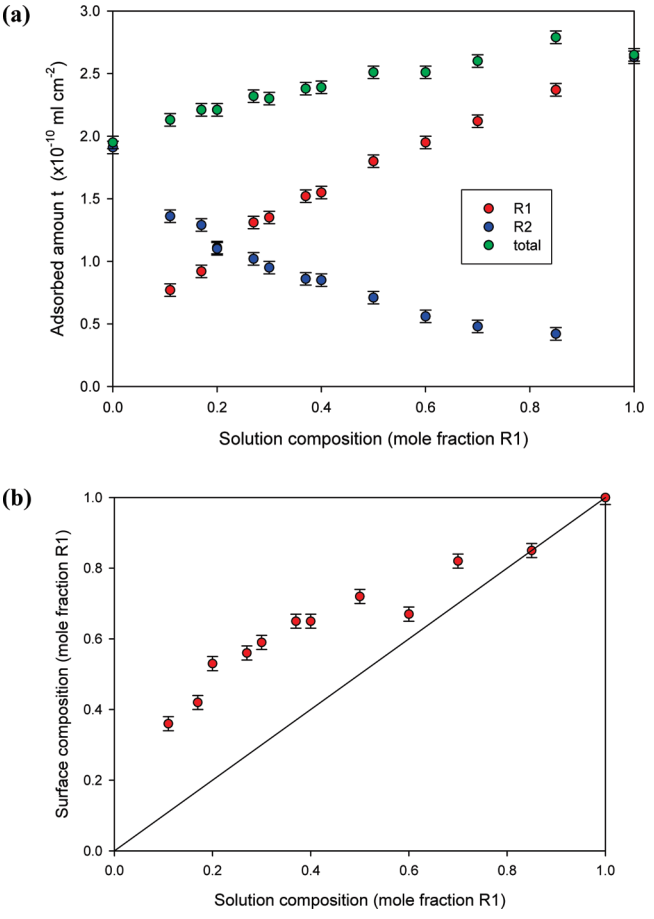


**Figure 6.** (a) Adsorption of R1, R2, and R1 + R2 for a 1 mM R1/R2 mixture at pH 9 (in buffer). (b) Surface composition (mole fraction of R1) vs solution composition at a surfactant concentration of 1 mM at pH 9 (in buffer) for the R1/R2 mixture. The solid line is a guide to the eye and represents the line of equal surface and solution composition.

Similar measurements were made for R1 and R2 separately at a solution concentration of 1 mM. In this case, eq 10 now contains only two terms, $\rho(z) = b_R n_R(z) + b_s n_s(z)$, and eq 11 becomes

$$R(Q) = \frac{16\pi^2}{Q^2}[b_R{}^2 h_{RR} + + b_s{}^2 h_{ss} + + 2b_R b_s h_{Rs}] \qquad (11)$$

From measurements for 1 mM R1 and 1 mM R2 for isotopic combinations d-R1(R2)/nrw, d-R1(R2)/$D_2O$, and h-R1(R2)/$D_2O$, the three partial structure factors for R1 and R2 (in eq 11) can be extracted. The resulting volume fraction distributions for the individual components are also plotted in Figure 7. The key model parameters from the analysis of the partial structure factors for R1, R2, and the R1/R2 mixture are summarized in Table 5.

The structural measurements presented here provide information about the distribution of rhamnolipids R1 and R2 and the associated solvent at the interface for R1 and R2 separately at 1 mM and for R1 and R2 in a 1 mM 70/30 mol/mol R1/R2 mixture. From the volume fraction distributions plotted in Figure 7 (the zero point in $z$ is arbitrarily chosen as the center of the surfactant distribution) and the model parameters summarized in Table 5, a number of key features are evident. First, the width of the surfactant distribution is approximately constant for R1 and R2 in the R1/R2 mixture, with a Gaussian width, $\sigma$, of about 17 Å. This value is comparable to those reported for other related surfactant systems,[19] and with the equivalent values quoted in Tables 3 and 4, where the adsorbed layer is modeled as a layer of uniform composition. The widths of the distributions for R1 and R2 are within error identical, and hence the conformation at the interface is such that the larger dirhamnose headgroup of R2 does not significantly alter the overall thickness of the adsorbed layer. This is in part masked by the capillary wave contribution to the overall thickness, which is typically about 9 Å in related systems.[19] This adds in quadrature to the intrinsic layer thickness and hence contributes about 2.5 Å to the total thickness. The second noteworthy feature is that the position of the surfactant distribution relative to the solvent, $\delta_{rs}$, is also relatively constant for the three measured structures and is about 7 Å. The main difference in the surface structures for R1 and R2 is the relative widths of the solvent distributions at the interface. The solvent distribution, $\xi_s$, for the R1/R2 mixture is broader than for the pure R1 and R2 monolayers, 7 Å compared with 5 and 3 Å for R1 and R2, and the solvent distribution for R2 is the narrowest at 3 Å. It is normally assumed[36] that the solvent at the interface is predominantly associated with the hydrophilic headgroup, and hence these differences can be in part be interpreted in terms of the headgroup conformation at the interface. This indicates that the dirhamonse headgroup of R2 is more compact (in the $z$ direction) than the smaller monorhamnose headgroup of R1. This implies a conformational change between R1 and R2 and less efficient lateral packing at the interface (hence the larger area/molecule for R2). In the R1/R2 mixture, the solvent distribution is broader than for R1 and R2 alone, and this implies that the optimal packing of R1 and R2 at the interface is associated with some induced disorder or staggered conformation of the two headgroups at the interface. Without a more detailed partial labeling of the individual surfactant components it is difficult to infer any more detailed structural information.

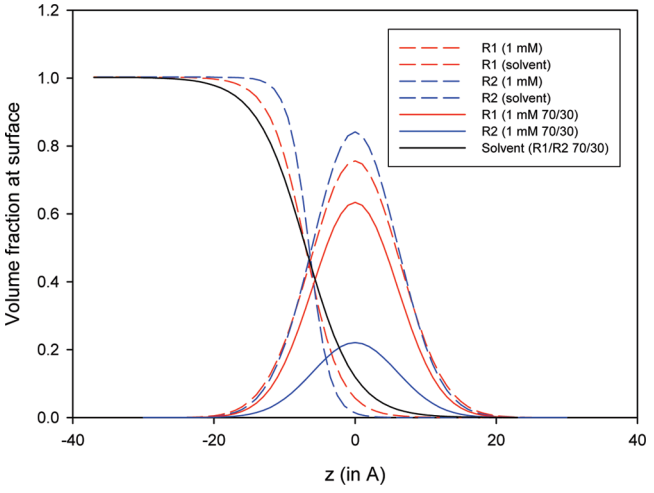


**Figure 7.** Volume fraction distributions for 1 mM R1, 1 mM R2, and 1 mM 30/70 R1/R2 at the interface from partial structure factor analysis.

**(2). Solution Self-Assembly.** (*i*). *R1, R2, and R1/R2 Mixtures*. The solution self-assembly and phase behavior for R1, R2, and the R1/R2 mixture in buffer at pH 9 have been derived from predominantly SANS measurements. Measurements for R1 and R2 were made in dilute solution from 20 to 100 mM. Measurements of the structure of the R1/R2 mixtures were made in the same concentration range and over a wide solution composition range. In this low-concentration range (as previously demonstrated in related surfactant systems[37−39]), SANS provides a sensitive and direct means of quantifying the associated phase behavior.

Figure 8 shows some typical SANS data for R2 at 20, 50, and 100 mM (Figure 8a), for R1 at 20, 30, 50, and 100 mM (Figure 7b), and for 60/40 R1/R2 at 20, 30, 40, 50, 70, and 90 mM (Figure 8c).

The SANS data for R2 at 20, 50, and 100 mM (Figure 8a) are characteristic of those obtained for relatively small globular micelles. With increasing surfactant concentration, the scattering intensity increases because of the higher micelle concentration and the formation of larger micelles. At the lower surfactant

**Table 5. Model Parameters from R1, R2, and R1/R2 and Partial Structure Factor Analysis**

(a) 1 mM R1, R2

| system | $\sigma_R$ (±1 Å) | $n$ (±0.03 × $10^{-3}$ Å$^{-3}$) | $A$ (±3 Å$^2$) | $\xi_s$ (±0.5 Å) | $\delta_{Rs}$ (±0.5 Å) |
|---|---|---|---|---|---|
| R1 | 18.0 | 0.93 | 68 | 5.0 | 7.0 |
| R2 | 17.0 | 0.8 | 83 | 3.0 | 6.5 |

(b) 1 mM 70/30 R1/R2

| $\sigma_{R1}$ (±1 Å) | $n_{R1}$(±0.03 × $10^{-3}$ Å$^{-3}$) | $A_{R1}$ (±3 Å$^2$) | $\sigma_{R2}$ (±1 Å) | $n_{R2}$ (±0.03 × $10^{-3}$ Å$^{-3}$) | $A_{R2}$(±10 Å$^2$) | $\xi_s$ (±0.5 Å) | $\delta_{R1s}$ (±0.5 Å) | $\delta_{R2s}$ (±0.5 Å) | $\delta_{R1R2}$ (±0.5 Å) |
|---|---|---|---|---|---|---|---|---|---|
| 17.0 | 0.7 | 85 | 17.0 | 0.21 | 316 | 7.0 | 7.0 | 7.0 | 0.0 |

concentrations, the micelles are only weakly interacting. The strength of that interaction increases slightly with increasing surfactant concentration, and is characterized by the slight suppression of the scattering intensity at low $Q$ values.

In the micellar regions of the phase diagram, the scattering has been analyzed quantitatively using a standard model for interacting globular micelles,[24] as described briefly in the Experimental Details section. A core + shell form factor is used to describe the micelle geometry in which molecular constraints are incorporated. It can be spherical or elliptical, depending upon the geometrical constraints. For spheres, the inner core, radius $r1$, containing the alkyl chains, is constrained to have a maximum dimension of the fully extended alkyl chain length, $l_c$, that is taken here to be 14.0 Å. This is modified by an additional factor, ext, that allows for additional packing constraints, some alkyl chain/headgroup mixing, and uncertainties in the actual alkyl chain/headgroup interface such that the inner core radius is $r1 \times$ ext. In this study, the parameter ext varies between 0.8 and 1.05 for the analysis of R2 micelles and R1/R2 mixed micelles. The outer radius $r2$ is defined by the outer shell that is determined by space filling of the shell volume with the headgroups and their associated hydration. For aggregation numbers, $\nu$, greater than that which can be accommodated in a spherical volume defined by a radius, $r1 = l_c$ ext, growth is accommodated by allowing the micelle shape to become elliptical. The ellipticity is defined be the parameter ee such that the overall dimensions are defined as $r2$, $r2$, and ee $r2$. In this study, the aggregation numbers are such that the globular micelles are always elliptical, with ee greater than 2.0. From known molecular volumes, scattering lengths (Table 2), and the total surfactant concentration, all of the parameters required for eqs 2 and 3 can be calculated. The refinable model parameters are then $\nu$, the surface charge, $z$ (which along with the micelle number density, $n$, defines the strength of the intermicellar interaction), and ext.

Table 6a summarizes the key model parameters for R2 at 20, 50, and 100 mM, which are typical of the range of parameters encountered in this study.

The standard core + shell model provides a good description of the micelle scattering data and has been applied here to the scattering data for R2 and R1/R2 mixtures that are micellar or predominantly micellar. In Table 6b, the variation in the micelle aggregation number with solution concentration and composition (R1/R2) obtained from this analysis is tabulated.

For R2 at the lowest surfactant concentration measured, the aggregation number is relatively low, about 30, but largely because of the packing constraints described earlier, the micelles are elliptical in shape. With increasing surfactant concentration, the pure R2 micelles grow such that at 100 mM the aggregation number is about 90 and the micelles are more anisotropic in shape (more elliptical). At a surfactant concentration of 20 mM, the solution microstructure is micellar, $L_1$, over the whole composition range, from pure R2 to pure R1 solutions. At this concentration, as the solution composition evolves from R2-rich to R1-rich compositions, the micelle aggregation number changes by a relatively modest factor of 2. For R2-rich R1/R2 compositions, from 100% R2 to 60% R2, which is still micellar, the micelle growth with increasing surfactant concentration is much more pronounced as the solution becomes richer in R1. For example, for 40/60 mol/mol R1/R2 at 100 mM the micelle aggregation number has increased by an order of magnitude, compared with its value at 20 mM. In summary, at the lowest surfactant concentrations the variation in the aggregation number with R1/R2 composition is relatively small and the aggregation number increases as the solution becomes richer in R1. At the higher surfactant concentrations, this variation is increasingly more pronounced with increasing concentration. This reflects the greater tendency of R1 to favor aggregates with lower curvature.

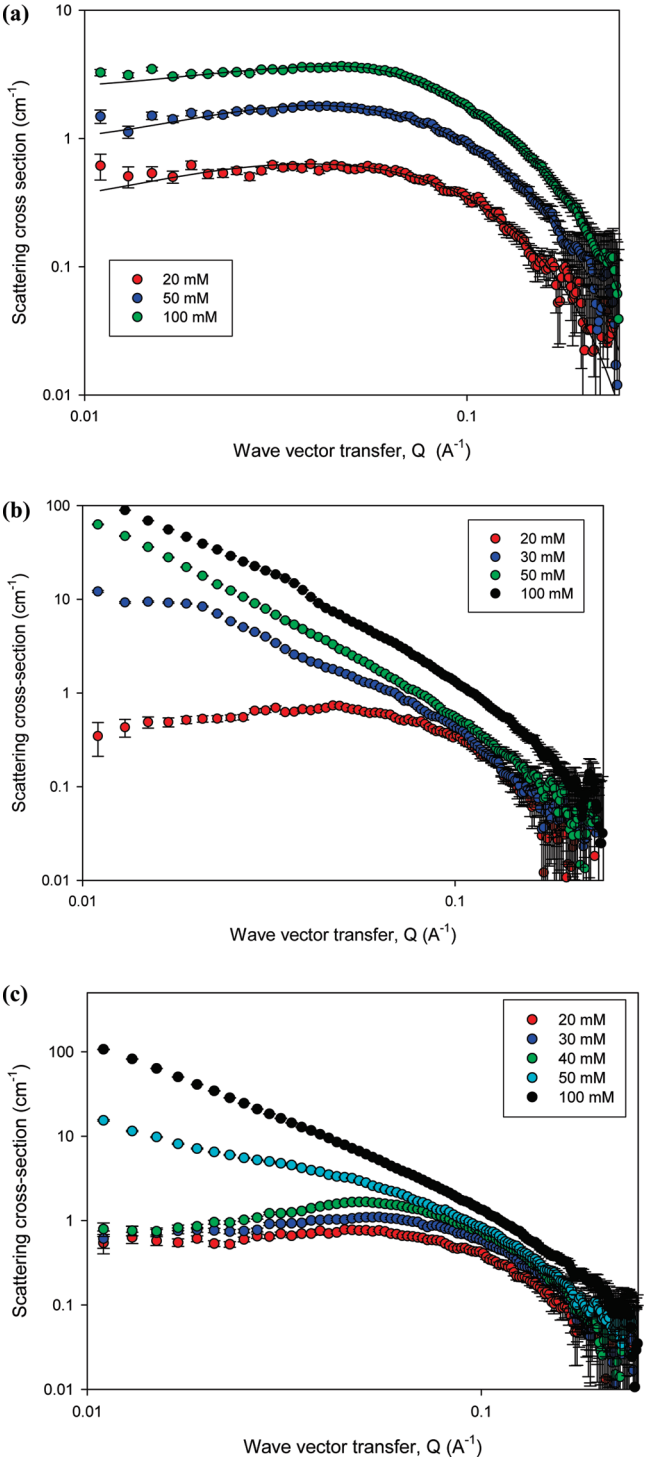


**Figure 8.** SANS scattering data. (a) Scattering cross-section (cm$^{-1}$) vs wave vector transfer, $Q$ (Å$^{-1}$), for 1 mM R2 at 20, 50, 100 mM. The solid lines are model fits as described in the text for globular micelles. Scattering cross-section (cm$^{-1}$) vs wave vector transfer, $Q$ (Å$^{-1}$), (b) for 1 mM R1 at 20, 30, 50, and 100 mM and (c) 60/40 mol/mol R1/R2 at 20, 30, 40, 50, and 100 mM.

(37) Tucker, I.; Penfold, J.; Thomas, R. K.; Grillo, I. *Langmuir* **2008**, *24*, 7674.
(38) Tucker, I.; Penfold, J.; Thomas, R. K.; Grillo, I.; Barker, J.; Milner, D. *Langmuir* **2008**, *24*, 6509.
(39) Tucker, I.; Penfold, J.; Thomas, R. K.; Grillo, I. *Langmuir* **2008**, *24*, 1863.

**Table 6. Model Parameters**

(a) Model Parameters from Micelle Model Analysis for 1 mM R2/$D_2O$ at pH 9 (in Buffer) at 20, 50, and 100 mM

| surfactant concentration (mM) | aggregation number, $\nu$, (±2) | surface charge, $z$, (±0.5) | R1 (±1 Å) | R2 (±1 Å) | ext (±0.5) | ee (±0.1) |
|---|---|---|---|---|---|---|
| 20 | 26 | 2.5 | 12.0 | 15.0 | 0.85 | 2.2 |
| 50 | 34 | 2.0 | 12.0 | 15.0 | 0.85 | 3.0 |
| 100 | 86 | 6.0 | 11.0 | 15.0 | 0.8 | 9.8 |

(b) Variation in Micelle Aggregation Number with Solution Concentration and Composition for R1 / R2

| concentration (mM) → composition (mole fraction of R2) | 20 (±2) | 30 | 40 | 50 | 60 | 100 |
|---|---|---|---|---|---|---|
| 1.0 | 26 | [a] | [a] | 34 | [a] | 86 ± 5 |
| 0.8 | 29 | [a] | [a] | 42 | [a] | 117 ± 10 |
| 0.6 | 33 | [a] | [a] | 51 | [a] | 310 ± 20 |
| 0.5 | 36 | [a] | [a] | [a] | 49 | [b] |
| 0.4 | 37 | 38 | 51 | [a] | 55 | [b] |
| 0.3 | 41 | 42 | 44 | [a] | [a] | [b] |
| 0.2 | 42 | 48 | [a] | [b] | [b] | [b] |
| 0.1 | 49 | [a] | [a] | [a] | [a] | [b] |
| 0.0 | 47 | [a] | [b] | [b] | [b] | [b] |

(c) Variation in Micelle Surface Charge with Solution Concentration and Composition for R1/R2

| concentration (mM) → composition (mole fraction of R2) | 20 (±2) | 30 | 40 | 50 | 60 | 100 |
|---|---|---|---|---|---|---|
| 1.0 | 2 | | | 2 | | 6 |
| 0.8 | 3 | | | 4 | | 7 |
| 0.6 | 3 | | | 4 | [a]* | 6 |
| 0.5 | 5 | | | 7 | 10 | |
| 0.4 | 5 | 5 | 7 | | 10 | |
| 0.3 | 4 | | | 10 | | |
| 0.2 | 6 | | | | | |
| 0.1 | 8 | | | | | |
| 0.0 | 5 | | | | | |

[a] Not measured or the $L_1/L_\alpha$ ($L_\alpha/L_1$) and $L_\alpha$ components are too large for reliable quantitative analysis. [b] $L_\alpha$ or predominantly $L_\alpha$ (Figure 9).

For R1-rich R1/R2 solution compositions, the form of the scattering is dramatically different, as illustrated in Figure 8b. At a surfactant concentration of 20 mM, the scattering (as discussed earlier) is still in the form of small globular micelles. At the higher surfactant concentrations (50 and 100 mM), the scattering has a different form and has a predominantly $Q^{-2}$ dependence. This form of the scattering dependence on $Q$ is consistent with the formation of planar lamellar structures, $L_\alpha$, in the form of large polydisperse vesicles. The lack of pronounced features in the $Q^{-2}$ dependence is consistent with relatively flexible membrane structures and hence must be large polydisperse ULV or BLV. The scattering pattern at a surfactant concentration of 30 mM is consistent with the coexistence of micelles and lamellar structures, and this is reflected in the phase behavior summarized in Figure 9. In the mixed $L_1/L_\alpha$ region, complementary light scattering measurements (Experimental Details) were used to define the mixed-phase boundaries more precisely.

At intermediate R1/R2 compositions, the evolution of the form of the scattering with increasing surfactant concentration is different again, and this is illustrated in Figure 8c for 60/40 mol/mol R1/R2. At the lower surfactant concentrations (20, 30, and 40 mM), the scattering is consistent with small globular micelles that show only a modest increase in size over that limited concentration range (Table 6b). At the highest surfactant concentration measured (100 mM), the scattering again has a $Q^{-2}$ dependence with no pronounced features. From previous discussions, this is also consistent with the formation of relatively large flexible vesicles (ULV and BLV). At the intermediate concentration (50 mM), the scattering is consistent with the coexistence of micellar and lamellar structures.

(*ii*). *Discussion*. The Israelachivili, Mitchell, and Ninham packing parameter, pp,[40] (where pp = $V/Al_c$ and $V$ is the alkyl chain volume, $l_c$ is the extended alkyl chain length, and $A$ is the area per molecule), based on geometrical packing arguments, has been very effective in predicting the general trends in the evolution of surfactant self-assembled structures. For pp < $^1/_3$, spherical micelles exist; for $^1/_3$ < pp < $^1/_2$, elongated micelles are formed; and for pp > $^1/_2$, planar structures exist. Here for R1 and R2 (from the known molecular volumes, from $l_c$, and from $A$ taken from the adsorption data; see Tables 1 and 3), values of pp = 0.67 and 0.5 for R1 and R2, respectively, are obtained. Except at the lowest concentration (20 mM), R1 is predominantly planar, which is consistent with the estimated pp value. However, for R2 the calculated pp values predict very elongated/planar structures, whereas over the concentration range measured, R2 is in the form of smaller globular micelles. To be consistent with the packing arguments, R2 would require an effective area per molecule of ~120 Å$^2$ (compared to 80 Å$^2$ from the adsorption data). This would imply that the packing constraints at the planar interface are different from those in the micelles and that in the micelles the R2 dirhamnose headgroup adopts a different conformation than at the air−water interface.

(40) Isrealachivili, J. N.; Mitchell, D. J.; Ninham, B. W. *J. Chem. Soc., Faraday Trans.* **1976**, *2*, 1525.

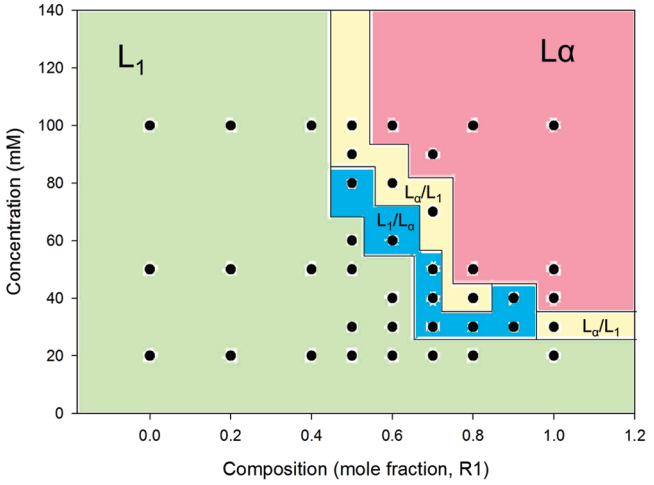


**Figure 9.** R1/R2 phase diagram (surfactant concentration vs surfactant composition) derived from SANS and light scattering data.

A notable feature of the quantitative analysis of the micelle scattering data is the relatively low values of the micelle surface charge, $z$. Expressed in terms of the degree of ionization of the micelles, $\delta = z/\nu$, it is $\leq 0.1$ for R2-rich solution compositions and increases to ~0.15 to 0.2 for R1-rich compositions. This is consistent with the deductions made on the basis of the surface tension measurements that R1 and R2 are only weakly ionic. Furthermore, these results indicate that R1 is slightly more ionic than R2, and this is consistent with the arguments of Guo et al.[14] regarding the conformation of the dirhamnose headgroup. For purely ionic surfactants, for example, SDS, the degree of micelle ionization is typically ~0.25 to 0.3.[24] Much lower values of $\delta$ and variations with solution composition for SDS/nonionic surfactant mixtures were reported by Penfold et al. [41] In that study, values of $\delta \leq 0.1$ were reported for SDS/$C_{12}E_6$ and SDS/$C_{12}E_8$ mixtures that were rich in the nonionic surfactant (>80 mol % nonionic). However, for solutions of >50/50 mol/mol SDS/nonionic mixtures the micelle surface charge was already similar to that for pure SDS micelles. These observations strongly reinforce the earlier deduction that the rhamnolipids, even at pH 9, are only weakly ionic.

The overall phase behavior deduced from the SANS and LS data for the R1/R2 mixture is summarized in Figure 9.

The structure of R2 aggregates, in dilute solution, is micellar ($L_1$) over the concentration range measured, and at the lowest surfactant concentration, R1 is also micellar. With increasing surfactant concentration, the structure of the R1 aggregates evolves from micellar to a more planar ($L_\alpha$) structure, either ULV or BLV. For the R1/R2 mixture, the structure of the R1-rich compositions at the higher surfactant concentrations is predominantly lamellar, whereas at the lowest surfactant concentration measured it is micellar over the entire composition range. For R2-rich compositions up to a solution composition of 40 mol % R1, mixed micelles exist. At intermediate R1/R2 compositions, there is a range of compositions where the solution is mixed phase; that is, lamellar and micellar structures coexist. This region can be further subdivided into regions where $L_1$ dominates and regions where $L_\alpha$ dominates, as illustrated in Figure 9. SANS measurements were used predominantly to determine the phase behavior. In the mixed-phase region (especially regions dominated by $L_1$), additional light scattering measurements were made (Experimental Details) and provided additional sensitivity for identifying the extent of the mixed-phase regions

(41) Penfold, J.; Tucker, I.; Thomas, R. K.; Staples, E.; Schuermann, R. *J. Phys. Chem. B* **2005**, *109*, 10760.

## 4. Summary

We have reported the use of surface tension and the neutron scattering techniques of SANS and NR to study solution self-assembly and adsorption at the air−water interface of rhamnolipids R1 and R2 and their mixtures. The deuterated and hydrogenated rhamnolipids used in this study were cultivated from a *Pseudomonas aeruginosa* culture and were separated and purified into their separate components.

At the air−water interface, R1 and R2 exhibit Langmuir-like adsorption isotherms with saturated area/molecule values of about 60 and 75 Å$^2$, respectively. In R1/R2 mixtures, there is a strong partitioning of R1 to the surface and R2 competes less favorably because of the steric or packing constraints of the larger R2 headgroup. A comparison of the ST and NR results show that the rhamnolipids are only weakly ionic species. Measurements of the structure of R1, R2, and the R1/R2 mixture at the air−water interface indicate that the position of the surfactant distribution relative to the solvent phase is unaltered in R1, R2, and the R1/R2 mixture. However, there are some systematic changes in the width of the solvent distribution that indicate a change in the headgroup conformation.

In dilute solutions (<20 mM), R1 and R2 form small globular micelles, $L_1$, with aggregation numbers of about 50 and 30, respectively. At higher concentrations, R1 has a predominantly planar structure, $L_\alpha$ (unilamellar or bilamellar vesicles), whereas R2 remains globular (with a modest increase in the aggregation number). For R1/R2 mixtures, solutions rich in R2 are predominantly micellar whereas solutions rich in R1 are planar. At intermediate compositions (60 to 80 mol % R1), there are mixed $L_\alpha/L_1$ and $L_1/L_\alpha$ regions. However, the higher preferred curvature associated with R2 tends to dominate the mixed R1/R2 phase behavior.

The quantitative analysis of the micellar scattering data indicates relatively small globular micelles that grow with increasing surfactant concentration and R1 content in the R1/R2 mixtures. From a comparison of the surface tension and neutron reflectivity adsorption data and the micelle degree of ionization extracted from the SANS data, the rhamnolipids are only weakly ionic, even at pH 9. It is also evident that R2 is less ionic in nature than R1, and this implies headgroup conformational changes that shield the charge on the carboxyl groups of the rhamnose units.

**Acknowledgment.** We acknowledge the provision of neutron beam time at ISIS (SURF, LOQ) and at the ILL (D11, D22) and the invaluable assistance of the instrument scientists at ISIS and the ILL. The support of Unilever and the dti Technology programme for the project is acknowledged.